BRILL

IAWA Journal 40 (1), 2019: 4–22

iawa

Large volume vessels are vulnerable to water-stress-induced embolism in stems of poplar

Anna L. Jacobsen[1,*], **R. Brandon Pratt**[1], **Martin D. Venturas**[2], and **Uwe G. Hacke**[3]

[1]Department of Biology, California State University, 9001 Stockdale Hwy, Bakersfield, CA 93311, U.S.A.
[2]School of Biological Sciences, University of Utah, 257S 1400E, Salt Lake City, UT 84112, U.S.A.
[3]Department of Renewable Resources, University of Alberta, Edmonton, AB T6G 2E3, Canada
*Corresponding author; email: ajacobsen@csub.edu

Accepted for publication: 21 November 2018

ABSTRACT

Xylem vessels interconnect to form the vessel network that is responsible for long-distance water transport through the plant. As plants dehydrate, the water column within vessels cavitates and gas emboli form, which block transport through embolized vessels. The impact of vessel blockages on transport through the xylem tissue depends upon vessel size and the arrangement and connections between vessels in the network. We examined if there was a correlation between vessel length and diameter within poplar stem xylem tissue using both silicone-injection and analysis of tissue volumes scanned using high-resolution computed tomography (microCT). We then used microCT to scan intact stems sampled over varying water potentials to examine if larger vessels, which would have the greatest impact on hydraulic transport, were more vulnerable to cavitation and embolism than smaller vessels. Within the xylem tissue, larger diameter vessels tended to be longer than narrow diameter vessels. Vessel size distributions indicated that most vessels were narrow and short, with fewer large vessels. Larger volume vessels tended to embolize at higher water potentials and the mean vessel volume of embolized vessels declined as water potentials declined. Hydraulic transport through the xylem tissue was near zero when about 40 % of the vessels within the xylem tissue volume were embolized, suggesting important vessel network effects occur as water moves through a three-dimensional (3D) tissue. The structure of the vessel network is important in understanding the impact of emboli within vessels on the overall hydraulic function of xylem tissue.

Keywords: Cavitation, cavitation resistance, embolism, HRCT, safety-efficiency tradeoff, vessel diameter, vessel length, vulnerability to cavitation.

Note: Supplementary material can be accessed in the online edition of this journal via brill.com/iawa.

DOI 10.1163/22941932-40190233

INTRODUCTION

Within angiosperm trees, long-distance water transport occurs through vessels within the xylem. Vessels are finite in length and water moves from one vessel to another through lateral pits as it traverses the relatively long transport distance of the root to leaf pathway. Across species, vessels vary in both their size and hydraulic function, including their conductive efficiency and ability to resist cavitation and embolism formation (Sperry *et al*. 2006). The arrangement of vessels with different hydraulic properties within the vessel network may also impact the function of xylem tissue as a whole (Venturas *et al*. 2016).

Vessel structure is linked to the hydraulic safety and efficiency of xylem tissue when examined across species. There is a strong relationship between vessel diameter and hydraulic transport as described by the Hagen-Poiseuille equation (Schulte *et al*. 1989). Vessel diameter has also been found to correlate to the vulnerability of vessels to water-stress-induced cavitation and embolism (reviewed in Hacke *et al*. 2017) and the relationship between vessel diameter and freezing-induced embolism is well known (Davis *et al*. 1999). Vessel length has been less studied than vessel diameter, but also appears to be linked to hydraulic transport efficiency and vulnerability to embolism when examined across species (Hacke *et al*. 2006; Lens *et al*. 2011; Jacobsen *et al*. 2016).

Within the xylem tissue, variation in the vulnerability of vessels to water-stress-induced cavitation and subsequent embolism formation has been hypothesized to be linked to differences in the sizes of vessels within the vessel network. The risk of vessel implosion is dependent on the thickness of the cell walls relative to the lumen diameter (Hacke *et al*. 2001). Large volume vessels may also have higher potential for air-seeding, because larger vessels contain more pitted wall area (Hargrave *et al*. 1994; Jarbeau *et al*. 1995; Wheeler *et al*. 2005; Christman *et al*. 2009, 2012). A study in aspen found that wider diameter vessels were more likely to embolize at higher (less negative) pressures than narrower diameter vessels, consistent with intra-tissue differences in vessel function (Cai & Tyree 2010), but differences in embolism vulnerability associated with vessel length and volume have not been previously evaluated within a tissue. This is at least partially due to the destructive sampling usually required to measure vessel length, which precludes simultaneous determination of vessel functional status. Intra-tissue and vessel-specific study of the relationship between vessel size and vulnerability is particularly important in identifying mechanisms of vessel vulnerability; these types of comparisons differ from those conducted across different individuals or species that rely on trait means for comparisons rather than the traits of specific vessels, although these studies are also useful in identifying correlations between vessel traits and hydraulic function (Olson *et al*. 2018).

Efforts to measure the three-dimensional (3D) structure of vessels in intact xylem have been facilitated by the application of high-resolution computed tomography (microCT; also referred to as HRCT) technology (Stuppy *et al*. 2003; Steppe *et al*. 2004). The combination of 3D structural information with the hydraulic status of vessels (*e.g*., gas vs. fluid-filled) (Vergeynst *et al*. 2014; Nardini *et al*. 2017) now permits studying the relationship between vessel size (length, diameter, volume) and function with-

in xylem tissue. In the present study, we used microCT to evaluate the sizes of vessels that were embolized at different water potentials. We evaluated the following questions:

What is the relationship between vessel diameter and length within stem xylem tissue? Across species, vessel length and diameter are not strongly correlated (reviewed in Jacobsen *et al*. 2012); however, within the tissue of an organ it appears that vessel diameter and length may be strongly correlated (Ewers & Fisher 1989; Liu *et al*. 2018). Understanding vessel length and diameter distributions is important for understanding the potential functional variability of vessels that co-occur within a tissue and that interact to form the vessel network.

Is vessel size (diameter, length, and volume) associated with differences in vulnerability to embolism of vessels within stem xylem tissue? As already discussed above, when analyzed across species, larger vessel diameters are correlated with increased vulnerability to embolism (reviewed in Hacke *et al*. 2017). Does this same pattern apply to understanding vessel function among co-occurring vessels within the xylem tissue? Are wider, longer, and larger vessels more vulnerable to embolism? This has implications for our understanding of xylem responses to water stress, in the interpretation of xylem vulnerability to embolism curves, and in potential differences in xylem hydraulic strategies in tissue with homogeneous versus heterogeneous vessel sizes.

MATERIALS AND METHODS

We sampled poplar trees (*Populus trichocarpa* Hook., Salicaceae) growing on campus in the Environmental Studies Area at California State University, Bakersfield, USA. Trees were grown in a well-watered field plot with trees spaced at 4 m increments along rows that were spaced 4 m apart (see Jacobsen *et al*. 2018 for additional plot information). Poplar trees were 11 years of age during the time of sampling in June to July 2018 and greater than 6 m in height. Poplar was selected for use in this study because of its relatively short vessel lengths, approximately 2 cm mean vessel length (Jacobsen *et al*. 2018), which allowed us to have many vessels start and end within the length of stem that we scanned using microCT. For all measures, fully illuminated current-year lateral branches from approximately 1.5 m above ground level were sampled. Samples were measured at approx. 0.35 m from branch apical meristems (Rosell *et al*. 2017).

Vessel diameter and length

We used two different methods to examine the relationship between vessel diameter and length, a silicone-injection method and microCT. For the silicone-injection method, six >1 m long branches were cut under water at predawn from different trees. Branches were transported from the field plot with their cut ends under water. In the lab, the proximal ends of branches were trimmed under water until a segment 35 cm in length, including the apical meristem, was obtained. The cut proximal end was trimmed carefully with a fresh razor blade under water and segments were mounted into a tubing system for silicone injection. Just prior to pressurization, the distal branch tip was trimmed with a razor blade to open the stem xylem at both sample ends. Segments were injected with a two-component silicone (RhodorsilRTV-141, Rhodia USA, Cran-

bury, NJ, USA) containing a UV stain (Uvitex OB, Ciba Specialty Chemicals, Basel, Switzerland) dissolved in chloroform (1% by weight). One drop of the UV stain was added per gram of silicone mixture. Segments were injected into their proximal end at 50 kPa for 24 h. After the injection, the segments were cured for at least 48 h at room temperature and then rehydrated prior to sectioning.

For determination of the vessel length distribution relative to the silicone-injection point, cross sections were obtained from the silicone-injection point (0.0 cm) and 0.7, 1.4, 2.9, 5.8, 11.8, and 24.0 cm from the injection point. For each cross section, the entire cross section was photographed under fluorescent light through a microscope attached to a digital camera (Zeiss Stereo Discover V.12 with Axiocam HRc digital camera, Carl Zeiss Microscopy, LLC, Thornwood, NY, USA). All silicone-filled vessels were counted at each sampled distance, representing total counts of 26,000 silicone-filled vessels across the six sampled stems. The mean vessel length was calculated from these counts using the equations reported by Sperry *et al*. (2005).

For determination of the relationship between vessel length and diameter, four higher-resolution images (100×) were captured from each cross section, taken in each of the four quadrants of each cross section and extending from the pith to the vascular cambium (Supplemental Online Material Fig. S1). The vessel lumen areas of all the silicone-filled vessels within these images were measured, including 14,478 total vessel diameters measured across the six sampled stems representing >50% of all silicone-filled vessels within each cross section. Vessel diameters were calculated from the measured lumen areas based on the assumption that vessels were circular. These values were used to calculate the mean vessel diameter of filled vessels at each sampling distance from the injection point. The relationship between distance from the injection point and vessel diameter was evaluated using linear regression (v. 17.2.1, Minitab, Inc., State College, Pennsylvania, USA).

Separate samples were evaluated for vessel length distribution as measured within a volume of xylem from stems scanned using microCT. Xylem stem segments, approximately 10 mm in length, were excised, in air, from the stems of 13 different trees at approximately 35 cm from the apical meristem, similar to the sample locations used for other measures. Each stem segment was air-dried by attaching it to tubing and pushing dry gas through the segment at 100 kPa for 5 min to fill all of the vessels within the segment with gas. This treatment rapidly dried samples and both vessels and non-living fibers filled with gas, including those that were not open at the ends of the samples. Following this treatment, we found that all of the vessels within the scanned segments were gas filled.

Segments were scanned using a microCT system (Bruker Corporation, Skyscan 2211, Billerica, MA, USA) at the CSUB Biology 3D Imaging Center. Scanned segments were 4.01 ± 0.12 mm (mean ± 1 SE) in diameter and we scanned each stem twice in adjacent areas and stitched the two scans together to create a longer scanned region (InstaRecon 1.7.3.0, InstaRecon Co., Champaign, IL, USA). The ultimate length of the scanned region was between 6.5 and 9 mm in length, depending on the amount of overlap between the two scanned regions. All scans were conducted at 3 μm resolution. The scan time for each sample was approximately 18 min. Using CTAn

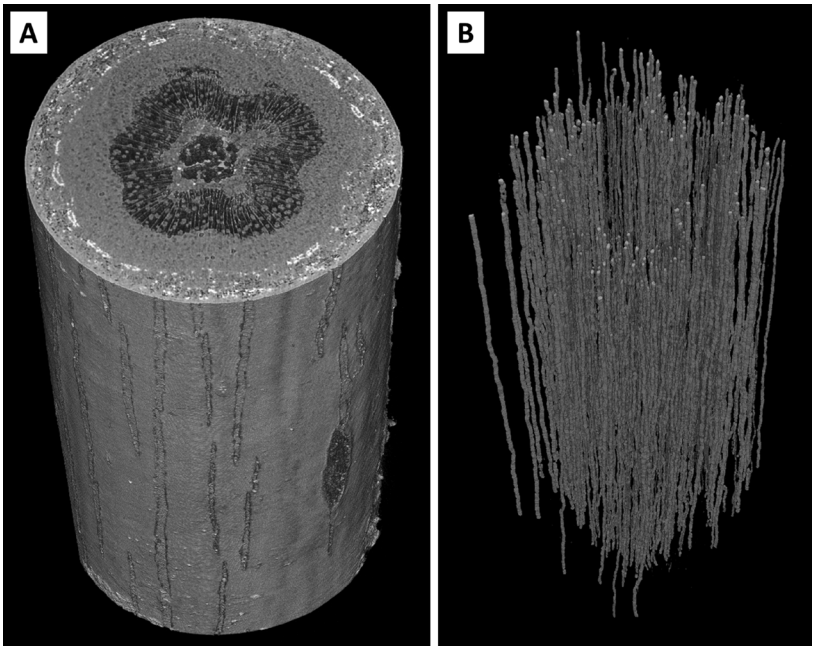

Figure 1. A representative poplar stem segment from the current study that was scanned using high resolution computed tomography (micro CT) to generate a 3D image of the stem, with cell walls and fluid visible as grey and gas as black (A). A 3D analysis of the xylem portion of the scanned stem was used to identify the gas-filled spaces within the xylem (vessel and fiber lumens) as objects that could then be further analyzed for their object dimensions (B). The gas-filled lumens from within the xylem as shown in panel B are from the stem sample shown in panel A.

software (Bruker Corporation, Billerica, MA, USA) we 3D filtered images using an anisotropic diffusion algorithm that removes noise and preserves edges. This helped to retain terminal vessel element walls. We analyzed a volume of interest in CTAn that included the xylem portions of each sample (excluding the bark and pith) (Fig. 1). A 3D object analysis evaluated all gas-filled spaces within the xylem (vessel and fiber lumens) and returned length and diameter measures for each object. For our samples, we used a minimum object length of 1200 μm, because this length corresponded to an upper limit for *P. trichocarpa* fibers from trees of similar size and age (1168 μm length reported for fibers in 9 yr old *P. trichocarpa* reported in Porth *et al*. 2013). In our samples, this length limit was found to be effective at removing most of the fiber lumens from the analysis, but also removed some of the smallest vessels. Since vessel elements averaged 270 μm in length (Jacobsen, unpublished data), this removed vessels that contained five or fewer vessel elements from the analysis. The remaining objects were assumed to represent gas-filled vessels.

For each 3D object identified from scans, we extracted information on the object length and diameter. For object diameter calculations, sphere-fitting was used to fill objects with the largest possible diameter spheres that would be contained within the object volume (Hildebrand & Rüegsegger 1997). Object diameter was then calculat-

ed as the average of the sphere diameters that were fit along the length of the object volume. In objects that are circular in cross section, the object diameter represents the true diameter, but as objects become less spherical, then this diameter underestimates the diameter relative to diameters calculated based on the lumen area as used in the cross-section analysis of the silicone-injected samples. All vessel-sized objects within the scanned volume were included in calculations of median vessel length. For evaluation of the relationship between object diameter and length, objects were limited to those that were shorter than 6400 μm, to remove objects that were longer than the scanned length, and to include only those that started and ended within the scanned segment. The relationship between object length and object diameter was evaluated using standardized major axis regression using an Excel worksheet (MS Excel, Bellingham, WA, USA).

Object diameters (*i.e.*, the mean diameter along the length of a vessel-sized object) were narrower than the diameters from cross-section analyses. This could be because of the incorporation of vessel taper and vessel diameter variation along the length of vessels (Akachuku 1987; Jupa *et al*. 2016) within this measure, because it is an average of the values along the whole length, or because vessels departed from being circular in cross section as described above. It is also possible that these values are smaller due to the taper of vessels as they approach the stem apex (Rosell *et al*. 2017). To ensure that this difference was not due to other measurement or calibration errors, we compared stem diameters and vessel diameters of matched samples using microCT, light microscopy, and caliper dimensions. In these comparisons, we found no difference between methods in stem dimension measures. The diameter of 3D objects and vessel diameters from light microscopy measures were highly correlated, with differences consistent with the calculation differences of these parameters as described above (Supplemental Online Material Fig. S2).

Vessel size and vulnerability to embolism

Large branches (> 2 m) were collected from the same trees used for the measures above at predawn (n = 15 branches). At least 4 leaves per branch were individually sealed within plastic bags and then the entire branches were placed within double plastic bags and transported to the laboratory to equilibrate for a minimum of 2 h. Trees were very hydrated at the time of sampling (predawn water potentials of ~-0.2 MPa) and scans of hydrated samples indicated that they contained no embolized vessels (Supplemental Online Material Fig. S3). Branches were taken out of bags to allow them to dehydrate to varying levels before being re-bagged and re-equilibrated in order to generate a range of water potentials. All branches were measured within one day of collection.

When branches were ready to be measured, water potential samples (4 leaves per branch) were removed from ~1 m from the branch apex and water potential was measured using a pressure chamber (PMS Instrument Company, Albany, OR, USA). The branch was then trimmed under water to a 0.50 m segment that terminated in the branch apex. The cut end of the branch was placed in a water-filled plastic tube and secured in place using plastic wrap. In addition, the entire branch was wrapped in plastic to prevent water loss or leaf movement during the scan. Branches were scanned using a

microCT system following the same procedure as described above and gas-filled objects within the xylem were analyzed in the same manner. The mean object diameter, length, and volume of the embolized vessels within each sample were calculated. The relationships between water potential and the sizes of embolized vessels were evaluated using Pearson correlation (v. 17.2.1, Minitab, Inc., State College, Pennsylvania, USA).

Following scanning, branches were removed from the microCT and transferred to a tub where they were trimmed under water to 0.14 m in length following the relaxation and cutting procedure described in Venturas *et al*. (2015). Stem segments were inserted into a conductivity system and their native hydraulic conductivity was measured gravimetrically using a conductivity apparatus under slight positive pressure (~2 kPa) using degassed ultra-filtered (in-line filter Calyx Capsule Nylon 0.1 μm, GE Water and Process Technologies, Trevose, PA, USA) 20 mM KCl solution. Maximum hydraulic conductivity was then measured on the same samples following a 1 h flush at 100 kPa using the same solution. Hydraulic conductivity measures were corrected for background flows measured at 0 kPa pressure (Hacke *et al*. 2000). The scanned regions of segments, approximately 1 cm long segments, were then excised, air-dried by pushing dry gas through the segment at 100 kPa for 5 min, and re-scanned using microCT as described above to determine the total number of vessels within the segment and to calculate the percentage of embolized conduits within the volume. The relationship between native hydraulic conductivity and the percentage of embolized conduits within the scanned 3D xylem tissue volume was examined using Pearson correlation.

Although not directly related to our experimental questions, we also calculated the water potential at 50 % loss in hydraulic conductivity (hydraulic samples) and the water potential at 50 % of vessels within the 3D volume embolized (microCT). These values are often used to estimate the hydraulic function of samples. For these calculations, each dataset was fit with a two parameter Weibull curve and 95 % confidence intervals were obtained via bootstrapping as specified in Hacke *et al*. (2015).

Some species may have vessels that are water-filled but that are not conductive either because they are still developing (Jacobsen *et al*. 2015) or because they are isolated from other conductive vessels due to emboli or other blockages (Pratt & Jacobsen 2018). Non-conductive water-filled vessels may complicate interpretation of microCT images if they are present. We tested for these potential issues in samples from our trees using three methods. One, we stained hydrated native samples for active xylem area (n = 9) using a 0.1 % (m/v) dye solution of crystal violet that was pulled up through the stems via transpiration from leaves. Dye was taken up through cut stem ends of samples ~ 0.50 m long for ~2 h. Stems were then thin sectioned by hand at 0.35 m from the stem apex using razor blades (GEM single-edge stainless steel PTFE-coated blades, Electron Microscopy Sciences, Hatfield, PA, USA) and mounted on slides in glycerol for anatomical observation. Two, samples (n = 15) were examined using fluorescence microscopy (Zeiss Stereo Discover V.12 with Axiocam HRc digital camera, Carl Zeiss Microscopy, LLC, Thornwood, NY, USA). These samples represented cross sections from all of the native stems used for the experiment described above. In the fluorescence images, differences in cell-wall chemistry and lignin content within the xylem appear

as differences in color, and immature xylem, when present, is visible as a band of different colored tissue near the cambium. Three, we feed an iodine solution (150 mM iohexol) up native cut branches (n = 3) following the methods in Pratt and Jacobsen (2018). Shoot segments were placed outside for 2–3.5 h to take up the iodine solution via transpiration. Then they were brought into the lab and prepared in the same way as other branches for microCT scanning.

Active xylem staining showed that vessels were conductive throughout the cross section, both near the vascular cambium and near the pith, and fluorescence images showed that the cell-wall chemistry of vessels was similar throughout the xylem and that there was no band of still developing xylem present (Supplemental Online Material Fig. S4 A–F). MicroCT scans of iodine feed samples showed that all water-filled vessels were conductive (Supplemental Online Material Fig. S4 G–I). Based on these tests, all vessels were considered potentially conductive in our analyses as the initial starting hydrated point for all samples.

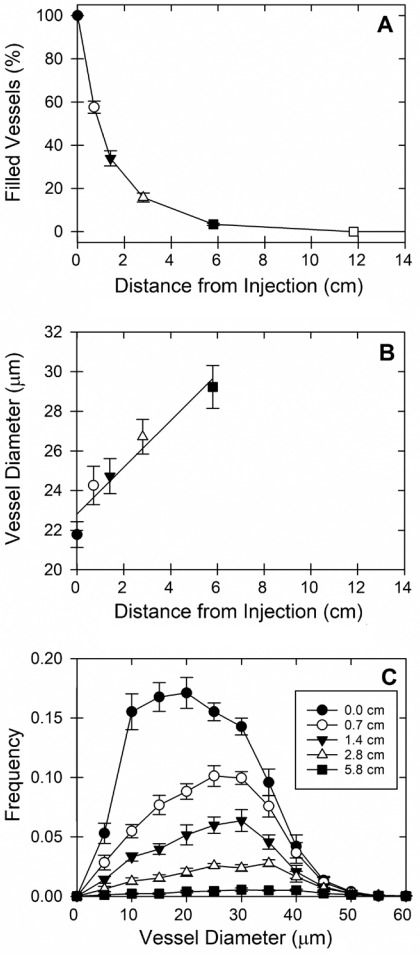

Figure 2. The proportion of vessels filled with silicone declined with increasing distance from the silicone injection point (A). Proportions are all relative to the number of vessels that were filled at the injection point (0.000 m). Longer vessels tended to be those with wider diameters (B). The mean vessel diameter of silicone-filled vessels increased with increasing distance from the silicone injection point as the vessels represented progressively longer size classes. The frequency of vessel diameter classes of silicone-filled vessels changed with increasing distance from the injection point (C). Frequencies are relative to the number of vessels that were filled at the injection point (0 cm). Each point in the figure above represents a mean ± 1 SE (n = 6 stems).

RESULTS

Longer vessels were wider in diameter

Vessel length analyses indicated that vessels in the poplar stem tissue that was examined were quite short. Median vessel length was 2.57 cm ± 0.19 (mean ± 1 SE, n = 6) based on the silicone-injection analysis, which represents the length distribution relative to the injection point. Median vessel length was 0.56 cm ± 0.08 (mean ± 1 SE, n = 13) based on the analysis of the distribution of vessel lengths within microCT scans of 3D volumes of xylem. The volume-based median was much shorter than the single-point injection median, in part, because many more short vessels may occur in a volume and this skews the volume-based distribution toward these more frequent short vessels.

For silicone-injected samples, the proportion of filled vessels declined rapidly with increasing distance from the injection point (Fig. 2A). Vessels that were longer (*i.e.*, filled for a greater distance from the injection point) had wider mean diameters relative to the mean of the vessels closer to the injection point (Fig. 2B). The mean vessel diameter at the injection point (*i.e.*, mean vessel diameter of all vessels) was 21.78 ± 0.66 μm (6 stem mean ± 1 SE; total vessels = 7021). Very few vessels were more than 5.8 cm in length and the mean diameter of these longest vessels was 29.24 ± 1.08 μm (6 stem mean ± 1 SE; total vessels = 40 at 5.8 cm). Only three of the six examined stems contained vessels that were longer than 11.8 cm (6 total vessels of the initial 7021 with a mean diameter of 44.98 ± 3.62 μm) and no vessels were longer than 24 cm. Vessel diameter was positively correlated with distance from the injection point (Fig. 2B; linear regression, $P = 0.007$, $r^2 = 0.934$, y-intercept = 22.819 ± 0.536, slope = 1.179 ± 0.181). These same patterns were apparent in the change in the frequency of vessel diameter size classes with increasing distance from the injection point (Fig. 2C), with vessel diameters becoming increasingly skewed toward larger diameters with increasing distance from the injection point. At the injection point, stems averaged 2064 ± 247 vessels within the injected cross section, with an average vessel density of 252.8 ± 21.4 (count mm^{-2}).

For microCT-scanned xylem tissue volumes, the frequency of vessels within different length classes declined rapidly (Fig. 3A), indicating that most vessels were quite short and that we were able to capture a large portion of the vessel length distribution with our samples. Vessels that were within the length classes that were analyzed (0.12–0.64 cm in length) represented the majority of vessels within samples, with 61.6% ± 6.52 (mean ± 1 SE) of all vessels occurring within this length range and the remaining vessels representing those that were longer than 0.64 cm (Fig. 3A inset). Vessels were wider in diameter in longer vessel length classes relative to shorter length classes (Fig. 3B). Vessel diameter and vessel length were positively correlated, although there was a large amount of variability in vessel diameter for a given vessel length (Fig. 3C; SMA regression, $P < 0.001$, $r = 0.150$, y-intercept = 8.022, slope*10^3 = 3.524, 95% confidence limits for slope*10^3 = 3.459–3.589). Across the analyzed vessels within the microCT- scanned volumes, mean vessel diameter was 15.84 ± 2.94 μm.

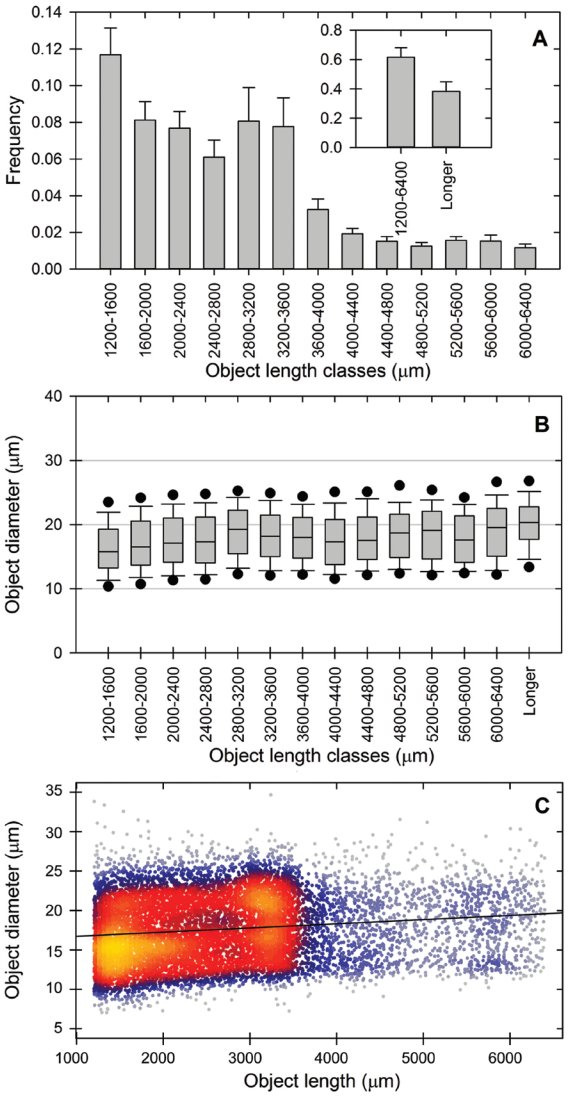

Figure 3. The size distribution of gas-filled objects within the xylem were examined from 3D microCT scans of xylem tissue, with results filtered to include objects that were consistent with the sizes of vessels. The decline in the number of objects within each length class corresponds to the vessel length distribution (A), with most vessels being relatively short (mean ± 1 SE, n = 13 stems). Objects that were 1200–6400 μm in length included most objects within scanned xylem samples (A inset). Vessel-sized objects were binned into 400 μm length classes and a box plot was generated for each class (B). For each box, the center line represents the median, the grey box represents 25 and 75 % data boundaries, the whiskers represent 10 and 90 % data boundaries, and black circles represent the 5 and 95 % data boundaries. Across all vessel-sized objects within the xylem there was a correlation between the length and diameter of objects (C). The colors in this panel correspond to the density of points, with yellow representing the greatest density of points, red intermediate, and blue low density.

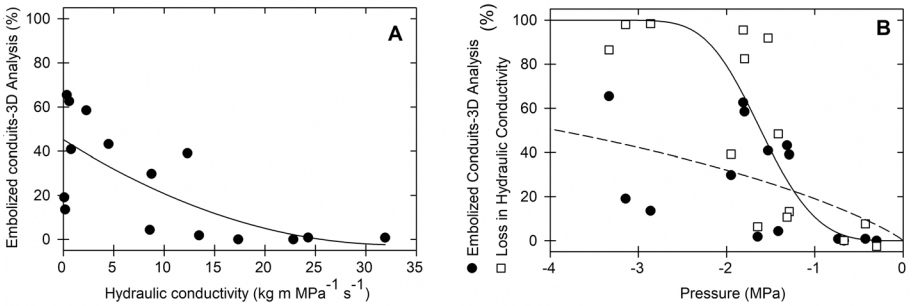

Figure 4. The proportion of embolized vessels within the xylem correlated with the hydraulic conductivity of samples (A). As pressure declined the percentage of embolized vessels within microCT scanned segments increased and the percentage loss of hydraulic conductivity also increased (B). Lines show the Weibull fit for the embolized conduits from 3D analysis of microCT scans (black circles and dashed line) and from hydraulic conductivity measures (open squares and solid line). Lines are shown only to assist with visual comparison of the data; see the Methods and Results for details of analyses. Each point represents a separate sample (n = 15 stems).

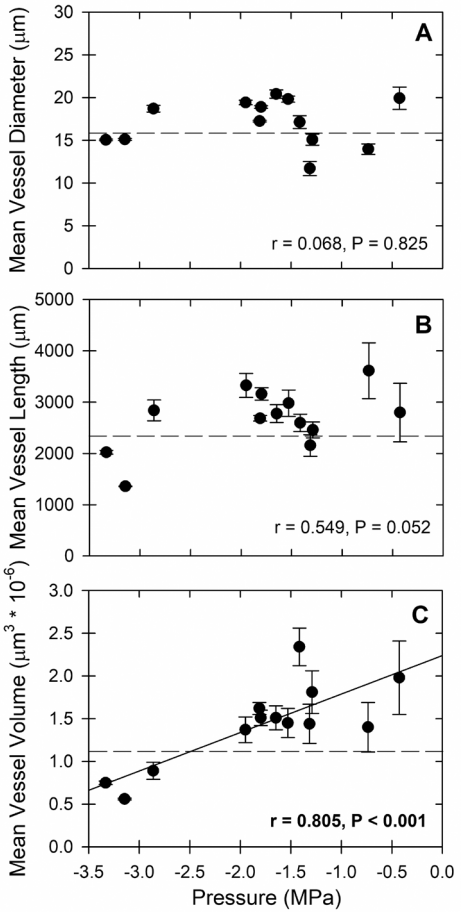

Figure 5. Mean vessel diameter (A), length (B), and volume (C) across stem samples of differing xylem water potential (pressure). Larger volume vessels tended to embolize at higher pressures and the mean vessel size declined with declining pressure as additional smaller vessels embolized (C). There was no correlation between mean vessel diameter (A) or mean vessel length (B) with pressure. Each panel shows the Pearson correlation and P value. The dashed line in each panel indicates the mean vessel size for each parameter based on the analysis of all vessels within scanned sections shown in Fig. 3. Each point represents a separate sample (mean ± 1 SE; n = 13 stems). Two hydrated stems from the experiment are not included in these analyses because they contained no embolized conduits.

Larger volume vessels embolized at higher (less negative) water potentials

The hydraulic conductivity of stem segments correlated with the proportion of embolized conduits within 3D scans of stem tissue (Fig. 4A), with lower conductivity correlated with an increasing number of embolized conduits (Pearson correlation, $P = 0.004$, $r = -0.700$). Samples that had little to no flow through the xylem (*i.e.*, hydraulic conductivity of 0) had approximately 40 % of their xylem vessels embolized (40.2 ± 13.8 %, n = 4 stems). No sample, even those that were severely dehydrated, exceeded 65 % of the vessels embolized within the scanned volume. As water potential declined, the proportion of embolized conduits within the xylem increased and the hydraulic conductivity of stem segments declined (Fig. 4B). The water potential at 50 % loss in hydraulic conductivity was -1.61 (-2.04 and -1.38 upper and lower 95 % confidence limits) and the water potential at 50 % of vessels embolized with the 3D tissue was -3.92 MPa (-6.66 and -1.98 upper and lower 95 % confidence limits).

Larger volume vessels tended to embolize at higher pressures. There was no correlation between mean vessel diameter or mean vessel length with pressure (Fig. 5A and 5B; Pearson correlation; $P > 0.05$ for both), but a size effect was apparent for mean vessel volume (Fig. 5C; Pearson correlation, $P < 0.001$, $r = 0.805$, n = 15 stems). Mean vessel volume of embolized vessels was highest in the most hydrated samples, indicating that the largest vessels within the samples were preferentially embolizing. In more dehydrated samples, more vessels were embolized (a higher %) and the mean vessel volume of these vessels declined indicating that smaller vessels were embolizing and this resulted in a reduction in the mean vessel diameter of the embolized conduits.

DISCUSSION

Vessel size distributions within xylem tissue

The xylem vessel network within current-year poplar stem xylem was composed of vessels that varied in their size distribution, including many small and narrow vessels and fewer longer and wider vessels. This result was supported using an established silicone-injection method (Sperry *et al*. 2005) and a microCT-based estimate of vessel length. To our knowledge, this is the first time that microCT has been used to evaluate vessel length distributions. Other studies have previously examined very short segments (~2 mm) to identify vessel endings (Wason *et al*. 2017) or very small xylem sectors (Brodersen *et al*. 2011), but neither of these studies examined the longer stem lengths included in this study (6.5–9.0 mm) that enabled us to develop vessel length distributions for the majority of vessels within scanned segments.

Median vessel lengths from scanned tissue volumes were shorter than those from silicone-based estimates of vessel length relative to the injection point. This is due to the strong skew toward small vessel lengths within volumes, where many small vessels may be packed into a volume relative to larger vessels. For example, the volume of 16 vessels of 10 μm in diameter and 1.2 mm in length is equal to the volume of one vessel 30 μm in diameter and 6.4 mm in length. This is important in understanding the structure of xylem; while the distribution of vessel lengths from a given point (*i.e.*, a cut end) may be important for some questions and studies, the volume-based distribution is

likely more important to our understanding of xylem function at the tissue level, which is the level that is most commonly measured. When examined at the tissue level, most vessels were quite short (less than 0.6 cm). Single-point injection-based estimates of vessel length distribution are biased toward longer vessels relative to what is present within the tissue as a whole and overestimate vessel length.

The widest diameter vessels within the stem xylem of poplar trees tended to be the longest vessels. This is consistent with several other studies that have measured vessel length and diameter and found that within the xylem tissue of an organ (*e.g.*, stems or roots) vessel length and diameter correlated (Ewers & Fisher 1989; Cai *et al.* 2010; Jacobsen *et al.* 2012, 2018; Liu *et al.* 2018). This within-tissue pattern may by a general feature of xylem within woody plants given the wide range of species, including trees, shrubs, and lianas, in which this pattern has now been described.

Within-tissue correlations between vessel diameter and length differ from across species relationships between these traits. Across species, in a global analysis, stem vessel length and diameter were only weakly correlated (reviewed in Jacobsen *et al.* 2012) and some species may have xylem that contains relatively long and narrow vessels (*e.g.*, Vander Willigen *et al.* 2000) or very wide and short vessels (Jacobsen *et al.* 2018). Vessel diameter and length also do not appear to be correlated when analyzed across organs. For instance, although roots of chaparral shrubs have wider vessels than stems (Pratt *et al.* 2007), roots do not have consistently longer vessel lengths (Pratt *et al.* 2015a). Similarly, poplar roots have much wider vessels than shoots, but vessel lengths were not different between these organs (Jacobsen *et al.* 2018). Thus, it is important to consider scale (tissue, organ, organisms, species) when extrapolating vessel size information based on diameter; while wide vessels may be longer within a tissue, there is less support for assumptions of diameter and length correlations across organs or species.

Large volume vessels and vulnerability to embolism

Large volume vessels were more likely to embolize at higher pressures than smaller vessels within poplar stems. This is consistent with the findings of Cai and Tyree (2010) within aspen stems, where they found that wider diameter vessels were more likely to embolize, although vessel diameter was not correlated with pressure in the present study. The within-tissue pattern of vessel size relating to vulnerability is consistent with the predictions of the 'rare pit hypothesis,' with large vessels containing more vessel wall area and more inter-vessel pits and therefore predicted to be more likely to contain a large and vulnerable pit membrane pore (Hargrave *et al.* 1994; Christman *et al.* 2009, 2012). In the present study, based on vessel size and our measured water potentials, it is unlikely that this size-dependent pattern in embolism risk was related to vessel implosion (Hacke *et al.* 2001).

The rate at which water is lost from cavitated vessels may affect our analysis of length and diameter. If the water in cavitated vessels drains slowly, recently cavitated vessels may take some time to fully embolize. In microCT scans, water at vessel termina and along vessel walls would make vessels appear smaller than they are, because this water would not be able to be visually resolved as separate from vessel walls. This

would presumably be more likely to occur in more hydrated samples that had recently embolized rather than in dehydrated samples that contained many vessels that had been cavitated for a longer period and would have had more time to form emboli and fully drain water from vessels. Importantly, the direction of this error would be in the opposite direction of what we observed and, if this were occurring, it would suggest an even larger vessel-size embolism risk than we found. This would not have affected vessel length and diameter measures in dried samples.

The shape of vulnerability to cavitation curves has been a topic of much recent interest (Cochard *et al*. 2010; Sperry *et al*. 2012; Wang *et al*. 2014; Cai *et al*. 2014) and it is worth considering how differential size-related vulnerability of vessels may relate to vulnerability curve shape. A sigmoidal curve with a steep slope indicates that most vessels are displaying a relatively similar vulnerability to cavitation; *i.e*., they embolize within a narrow pressure range. In contrast, other curve shapes, such as a linear or exponential with a long tail, indicate populations of vessels that differ in their cavitation resistance and that are cavitating across a range of differing pressures. For example, the xylem of ring-porous species, such as oak, is classically viewed as having a dual conducting system with large earlywood vessels that function when conditions are most favorable and that embolize early during the vulnerability curve (Christman *et al*. 2012; Venturas *et al*. 2016) and resistant small latewood vessels as well as tracheids (Pratt *et al*. 2017b) that function even when conditions are suboptimal (Sperry *et al*. 1994). Indeed, there may be an advantage to having a population of vulnerable vessels, such as the contribution of vessel water to capacitance (Vergeynst *et al*. 2014; Pratt & Jacobsen 2017; Rosner *et al*. 2018) or high transport capacity during brief periods when conditions are favorable (Taneda & Sperry 2008). The relationship between curve shape and vessel size distribution may be a particularly interesting area of future research.

The within-tissue correlation that we found between vessel size and vulnerability also has been found in studies that have looked across species. Many inter-specific studies have found correlations between vessel diameter and/or length and vulnerability to embolism (*e.g*., Hargrave *et al*. 1994; Martínez-Vilalta *et al*. 2002; Wheeler *et al*. 2005; Hacke *et al*. 2006; Jacobsen *et al*. 2007; Markesteijn *et al*. 2011; Lens *et al*. 2011; Olson *et al*. 2018). These studies found correlations between vessel dimensions and vulnerability to cavitation when comparing vulnerability curves based on flushed maximum values to mean tissue vessel dimensions, so hydraulics and anatomical measures would have included the same vessel population (*i.e*., most of the vessels). The findings of these studies contrast with a recent study (Lobo *et al*. 2018); however, this study measured unflushed xylem samples that had been stored for up to three weeks prior to vulnerability curve determination and they do not report information, such as native embolism or staining, on what population of vessels remained functional and were included in these measures. Similarly, Scholz *et al*. (2013) found that vessel dimensions were not correlated with cavitation resistance, but they used unflushed cavitron curves from Cochard *et al*. (2008) for their analysis, which would similarly exclude many vessels from functional measures leading to a discrepancy between the sampled vessel populations used to determine anatomy and functional traits. While

flushing may not be appropriate for all studies (see discussion in Sperry *et al*. 2012), studies on unflushed material are difficult to evaluate without information on the vessels that are active and the anatomical sampling of only those vessels that are active. To date, this type of analysis has been relatively rare (however, see Hargrave *et al*. 1994).

Vessel diameter, though often used as a proxy for vessel size, may not always be a strong predictor of vessel volume. The lack of a correlation between vessel diameter and vessel length (Ewers *et al*. 1990; Wheeler *et al*. 2005; Jacobsen *et al*. 2012) across some species may lead to vessel diameter not correlating to vessel volume, which would make vessel diameter unlikely to capture increased vulnerability of large volume vessels. This pattern was found in the present study, with vessel diameter changes not capturing vessel volume well due to the high variability of diameters for a given vessel length. Additionally, diameter *per se* is not necessarily correlated with the total area of inter-vessel pit membranes per conduit, which is one of the proposed mechanistic links between vessel size and vulnerability to cavitation; vessel volume is a better indicator of total pit area than vessel diameter.

Vessel network traits and conductivity

An interesting result from the present study is the relationship between the proportion of embolized vessels within the xylem tissue and the impact that these blockages have on flow. We found that extremely dehydrated stem samples, which had limited to no measurable flow through xylem segments, still had fluid in about 60 % of their vessels in microCT images. This result is similar to a recent study that found hydraulics-based percent loss in conductivity (PLC) greater than microCT-based estimates in dehydrated stems (Nolf *et al*. 2017); however, their 2D microCT data are different from ours, which were estimated on a 3D volume basis.

The underestimate of PLC by microCT data appears to be a pattern that is emerging in multiple independent studies (Jacobsen & Pratt 2018). One explanation for this pattern is that visual information on the proportion and structure of fluid-filled vessels in microCT analyses is not easily translated into tissue-level hydraulic conductivity for some species. A recent study by Mrad *et al*. (2018) found that 40–60 % of the vessels would still contain water when flows were reduced to less than the 10 % of the initial value, very similar to the value that we found within the present study. This model was based on the xylem traits of *Acer*, which also is diffuse porous with relatively short vessel lengths, similar to the poplar xylem examined in the present study. This suggests that incorporation of vessel network traits may be important in developing methods for microCT analysis that are able to accurately predict xylem function and in properly interpreting the functional implications of visual data.

ACKNOWLEDGMENTS

NSF HRD-1547784 (ALJ and RBP) and NSF Career Grant IOS-1252232 (ALJ) are acknowledged for support. Department of Defense (Army Research Office) proposal No. 68885-EV-REP and contract No. W911NF-16-1-0556 (RBP) is gratefully acknowledged. MDV was supported by NSF IOS-1450650. UGH acknowledges support from and NSERC Discovery grant.

REFERENCES

Akachuku AE. 1987. A study of lumen diameter variation along the longitudinal axis of wood vessels in *Quercus rubra* using cinematography. IAWA J. 8: 41–45. https://doi.org/10.1163/22941932-90001023.

Brodersen CR, Lee EF, Choat B, Jansen S, Phillips RJ, Shackel KA, McElrone AJ, Matthews MA. 2011. Automated analysis of three-dimensional xylem networks using high-resolution computed tomography. New Phytol. 191: 1168–1179. https://doi.org/10.1111/j.1469-8137.2011.03754.x.

Cai J, Li S, Zhang H, Zhang S, Tyree MT. 2014. Recalcitrant vulnerability curves: methods of analysis and the concept of fibre bridges for enhanced cavitation resistance. Plant Cell Environ. 37: 35–44. https://doi.org/10.1111/pce.12120.

Cai J, Tyree MT. 2010. The impact of vessel size on vulnerability curves: data and models for within species variability in saplings of aspen, *Populus tremuloides* Michx. Plant Cell Environ. 33: 1059–1069. https://doi.org/10.1111/j.1365-3040.2010.02127.x.

Cai J, Zhang S, Tyree MT. 2010. A computational algorithm addressing how vessel length might depend on vessel diameter. Plant Cell Environ. 33: 1234–1238. https://doi.org/10.1111/j.1365-3040.2010.02142.x.

Christman MA, Sperry JS, Adler FR. 2009. Testing the 'rare pit' hypothesis for xylem cavitation resistance in three species of *Acer*. New Phytol. 182: 664–674. https://doi.org/10.1111/j.1469-8137.2009.02776.x.

Christman MA, Sperry JS, Smith DD. 2012. Rare pits, large vessels and extreme vulnerability to cavitation in a ring-porous tree species. New Phytol. 193: 713–720. https://doi.org/10.1111/j.1469-8137.2011.03984.x.

Cochard H, Barigah ST, Kleinhentz M, Eshel A. 2008. Is xylem cavitation resistance a relevant criterion for screening drought resistance among *Prunus* species? New Phytol. 165: 976–982. https://doi.org/10.1016/j.jplph.2007.07.020.

Cochard H, Herbette S, Barigah T, Badel E, Ennajeh M, Vilagrosa A. 2010. Does sample length influence the shape of xylem embolism vulnerability curves? A test with the Cavitron spinning technique. Plant Cell Environ. 33: 1543–1552. https://doi.org/10.1111/j.1365-3040.2010.02163.x.

Davis SD, Sperry JS, Hacke UG. 1999. The relationship between xylem conduit diameter and cavitation caused by freezing. Am. J. Bot. 86: 1367–1372. https://doi.org/10.2307/2656919.

Ewers FW, Fisher JB. 1989. Variation in vessel length and diameter in stems of six tropical and subtropical lianas. Am. J. Bot. 76: 1452–1459. https://doi.org/10.1002/j.1537-2197.1989.tb15126.x.

Ewers FW, Fisher JB, Chiu ST. 1990. A survey of vessel dimensions in stems of tropical lianas and other growth forms. Oecologia 84: 544–552. https://doi.org/10.1007/BF00328172.

Hacke UG, Sperry JS, Pittermann J. 2000. Drought experience and cavitation resistance in six shrubs from the Great Basin, Utah. Basic Appl. Ecol. 1: 31–41. https://doi.org/10.1078/1439-1791-00006.

Hacke UG, Sperry JS, Pockman WT, Davis SD, McCulloh KA. 2001. Trends in wood density and structure are linked to prevention of xylem implosion by negative pressure. Oecologia 126: 57–461. https://doi.org/10.1007/s004420100628.

Hacke UG, Sperry JS, Wheeler JK, Castro L. 2006. Scaling of angiosperm xylem structure with safety and efficiency. Tree Physiol. 26: 689–701. https://doi.org/10.1093/treephys/26.6.689.

Hacke UG, Spicer R, Schreiber SG, Plavcová L. 2017. An ecophysiological and developmental perspective on variation in vessel diameter. Plant Cell Environ. 40: 831–845. https://doi.org/10.1111/pce.12777.

Hacke UG, Venturas MD, MacKinnon ED, Jacobsen AL, Sperry JS, Pratt RB. 2015. The standard centrifuge method accurately measures vulnerability to cavitation curves of long-vesselled olive stems. New Phytol. 205: 116–127. https://doi.org/10.1111/nph.13017.

Hargrave KR, Kolb KJ, Ewers FW, Davis SD. 1994. Conduit diameter and drought-induced embolism in *Salvia mellifera* Greene (Labiatae). New Phytol. 126: 695–705. https://doi.org/10.1111/j.1469-8137.1994.tb02964.x.

Hildebrand T, Rüegsegger P. 1997. A new method for the model-independent assessment of thickness in three-dimensional images. J. Microsc. 185: 67–75. https://doi.org/10.1046/j.1365-2818.1997.1340694.x.

Jacobsen AL, Pratt RB. 2018. Going with the flow: Structural determinants of vascular tissue transport efficiency and safety. Plant Cell Environ. 41: 2715–2717. https://doi.org/10.1111/pce.13446.

Jacobsen AL, Pratt RB, Davis SD, Ewers FW. 2007. Cavitation resistance and seasonal hydraulics differ among three arid Californian plant communities. Plant Cell Environ. 30: 1599–1609. https://doi.org/10.1111/j.1365-3040.2007.01729.x.

Jacobsen AL, Pratt RB, Tobin MF, Hacke UG, Ewers FW. 2012. A global analysis of xylem vessel length in woody plants. Am. J. Bot. 99: 1583–1591. https://doi.org/10.3732/ajb.1200140.

Jacobsen AL, Rodriguez-Zaccaro FD, Lee TF, Valdovinos J, Toschi HS, Martinez JA, Pratt RB. 2015. Grapevine xylem development, architecture and function. In: Hacke UG (ed.), Functional and ecological xylem anatomy: 133–162. Springer. https://doi.org/10.1007/978-3-319-15783-2_5.

Jacobsen AL, Tobin MF, Toschi HS, Percolla MI, Pratt RB. 2016. Structural determinants of increased susceptibility to dehydration-induced cavitation in post-fire resprouting chaparral shrubs. Plant Cell Environ. 39: 2473–2485. https://doi.org/10.1111/pce.12802.

Jacobsen AL, Valdovinos-Ayala J, Rodriguez-Zaccaro FD, Hill-Crim MA, Percolla MI, Venturas MD. 2018. Intra-organismal variation in the structure of plant vascular transport tissues in poplar trees. Trees-Struct. Funct. 32: 1335–1346. https://doi.org/10.1007/s00468-018-1714-z.

Jarbeau JA, Ewers FW, Davis SD. 1995. The mechanism of water-stress-induced embolism in two species of chaparral shrubs. Plant Cell Environ. 18: 189–196. https://doi.org/10.1111/j.1365-3040.1995.tb00352.x.

Jupa R, Plavcová L, Flamiková B, Gloser V. 2016. Effects of limited water availability on xylem transport in liana *Humulus lupulus* L. Environ. Exper. Bot. 130: 22–32. https://doi.org/10.1016/j.envexpbot.2016.05.008.

Lens F, Sperry JS, Christman MA, Choat B, Rabaey D, Jansen S. 2011. Testing hypotheses that link wood anatomy to cavitation resistance and hydraulic conductivity in the genus *Acer*. New Phytol. 190: 709–723. https://doi.org/10.1111/j.1469-8137.2010.03518.x.

Liu M, Pan R, Tyree MT. 2018. Intra-specific relationship between vessel length and vessel diameter of four species with long-to-short species-average vessel lengths: further validation of the computation algorithm. Trees 32: 51–60. https://doi.org/10.1007/s00468-017-1610-y.

Lobo A, Torres-Ruiz JM, Burlett R, Lemaire C, Parise C, Francioni C, Truffaut L, Tomášková I, Hansen JK, Kjær ED, Kremer A. 2018. Assessing inter- and intraspecific variability of xylem vulnerability to embolism in oaks. For. Ecol. Manage. 424: 53–61. https://doi.org/10.1016/j.foreco.2018.04.031.

Markesteijn L, Poorter L, Paz H, Sack L, Bongers F. 2011. Ecological differentiation in xylem cavitation resistance is associated with stem and leaf structural traits. Plant Cell Environ. 34: 137–148. https://doi.org/10.1111/j.1365-3040.2010.02231.x.

Martínez-Vilalta J, Prat E, Oliveras I, Piñol J. 2002. Xylem hydraulic properties of roots and stems of nine Mediterranean woody species. Oecologia 133: 19–29. https://doi.org/10.1007/s00442-002-1009-2.

Mrad A, Domec J-C, Huang C-W, Frederic L, Katul G. 2018. A network model links wood anatomy to xylem tissue hydraulic behaviour and vulnerability to cavitation. Plant Cell Environ. 41: 2718–2730. https://doi.org/10.1111/pce.13415.

Nardini A, Savi T, Losso A, Petit G, Pacilè S, Tromba G, Mayr S, Trifilò P, Lo Gullo MA, Salleo S. 2017. X-ray microtomography observations of xylem embolism in stems of *Laurus nobilis* are consistent with hydraulic measurements of percentage loss of conductance. New Phytol. 213: 1068–1075. https://doi.org/10.1111/nph.14245.

Nolf M, Lopez R, Peters JM, Flavel RJ, Koloadin LS, Young IM, Choat, B. 2017. Visualization of xylem embolism by X-ray microtomography: a direct test against hydraulic measurements. New Phytol. 214: 890–898. https://doi.org/10.1111/nph.14462.

Olson ME, Soriano D, Rosell JA, Anfodillo T, Donoghue MJ, Edwards EJ, León-Gómez C, Dawson T, Camarero Martínez JJ, Castorena M, Echeverría A, Espinosa CI, Fajardo A, Gazol A, Isnard S, Lima RS, Marcati CR, Méndez-Alonzo R. 2018. Plant height and hydraulic vulnerability to drought and cold. Proc. Nat. Acad. Sci. 115: 7551–7556. DOI: 10.1073/pnas.1721728115.

Porth I, Klápště J, Skyba O, Lai BS, Geraldes A, Muchero W, Tuskan GA, Douglas CJ, El-Kassaby YA, Mansfield SD. 2013. *Populus trichocarpa* cell wall chemistry and ultrastructure trait variation, genetic control and genetic correlations. New Phytol. 197: 777–790. https://doi.org/10.1111/nph.12014.

Pratt RB, Jacobsen AL. 2017. Conflicting demands on angiosperm xylem: tradeoffs among storage, transport, and biomechanics. Plant Cell Environ. 40: 897–913. https://doi.org/10.1111/pce.12862.

Pratt RB, Jacobsen AL. 2018. Identifying which conduits are moving water in woody plants: A new HRCT-based method. Tree Physiol. 38: 1200–1212. https://doi.org/10.1093/treephys/tpy034.

Pratt RB, Jacobsen AL, Ewers FW, Davis SD. 2007. Relationships among xylem transport, biomechanics, and storage in stems and roots of nine Rhamnaceae species of the California chaparral. New Phytol. 174: 787–798. https://doi.org/10.1111/j.1469-8137.2007.02061.x.

Pratt RB, MacKinnon ED, Venturas MD, Crous CJ, Jacobsen AL. 2015a. Root resistance to cavitation is accurately measured using a centrifuge technique. Tree Physiol. 35: 185–196. https://doi.org/10.1093/treephys/tpv003.

Pratt RB, Percolla MI, Jacobsen AL. 2015b. Integrative xylem analysis of chaparral shrubs. In: Hacke UG (ed.), Functional and ecological xylem anatomy: 189–207. Springer. https://doi.org/10.1007/978-3-319-15783-2_7.

Rosell JA, Olson ME, Anfodillo T. 2017. Scaling of xylem vessel diameter with plant size: causes, predictions, and outstanding questions. Current Forestry Reports 3: 46–59. https://doi.org/10.1007/s40725-017-0049-0.

Rosner S, Heinze B, Savi T, Dalla-Salda G. 2018. Prediction of hydraulic conductivity loss from relative water loss: new insights into water storage of tree stems and branches. Physiol. Plant. https://doi.org/10.1111/ppl.12790.

Scholz A, Rabaey D, Stein A, Cochard H, Smets E, Jansen S. 2013. The evolution and function of vessel and pit characters with respect to cavitation resistance across 10 *Prunus* species. Tree Physiol. 33: 684–694. https://doi.org/10.1093/treephys/tpt050.

Schulte PJ, Gibson AC, Nobel PS. 1989. Water flow in vessels with simple or compound perforation plates. Ann. Bot. 64: 171–178. https://doi.org/10.1093/oxfordjournals.aob.a087822.

Sperry JS, Christman MA, Torres-Ruiz JM, Taneda H, Smith DD. 2012. Vulnerability curves by centrifugation: is there an open vessel artefact, and are 'r'shaped curves necessarily invalid? Plant Cell Environ. 35: 601–610. https://doi.org/10.1111/j.1365-3040.2011.02439.x.

Sperry JS, Hacke UG, Pittermann J. 2006. Size and function in conifer tracheids and angiosperm vessels. Am. J. Bot. 93: 1490–1500. https://doi.org/10.3732/ajb.93.10.1490.

Sperry JS, Hacke UG, Wheeler JK. 2005. Comparative analysis of end wall resistivity in xylem conduits. Plant Cell Environ. 28: 456–465. https://doi.org/10.1111/j.1365-3040.2005.01287.x.

Sperry JS, Nichols KL, Sullivan JEM, Eastlack SE. 1994. Xylem embolism in ring-porous, diffuse-porous, and coniferous trees of Northern Utah and Interior Alaska. Ecology 75: 1736–1752. https://doi.org/10.2307/1939633.

Steppe K, Cnudde V, Girard C, Lemeur R, Cnudde JP, Jacobs P. 2004. Use of X-ray computed microtomography for non-invasive determination of wood anatomical characteristics. J. Struct. Biol. 148: 11–21. https://doi.org/10.1016/j.jsb.2004.05.001.

Stuppy WH, Maisano JA, Colbert MW, Rudall PJ, Rowe TB. 2003. Three-dimensional analysis of plant structure using high-resolution X-ray computed tomography. Trends Plant Sci. 8: 2–6. https://doi.org/10.1016/S1360-1385(02)00004-3.

Taneda H, Sperry JS. 2008. A case-study of water transport in co-occurring ring- versus diffuse-porous trees: contrasts in water-status, conducting capacity, cavitation and vessel refilling. Tree Phys. 28: 1641–1651. https://doi.org/10.1093/treephys/28.11.1641.

Vander Willigen C, Sherwin HW, Pammenter NW. 2000. Xylem hydraulic characteristics of subtropical trees from contrasting habitats grown under identical environmental conditions. New Phytol. 145: 51–59. https://doi.org/10.1046/j.1469-8137.2000.00549.x.

Venturas MD, MacKinnon ED, Jacobsen AL, Pratt RB. 2015. Excising stem samples underwater at native tension does not induce xylem cavitation. Plant Cell Environ. 38: 1060–1068. https://doi.org/10.1111/pce.12461.

Venturas MD, Rodriguez-Zaccaro FD, Percolla MI, Crous CJ, Jacobsen AL, Pratt RB. 2016. Single vessel air injection estimates of xylem resistance to cavitation are affected by vessel network characteristics and sample length. Tree Physiol. 36: 1247–1259. https://doi.org/10.1093/treephys/tpw055.

Vergeynst LL, Dierick M, Bogaerts JA, Cnudde V, Steppe K. 2014. Cavitation: a blessing in disguise? New method to establish vulnerability curves and assess hydraulic capacitance of woody tissues. Tree Physiol. 35: 400–409. https://doi.org/10.1093/treephys/tpu056.

Wang R, Zhang L, Zhang S, Cai J, Tyree MT. 2014. Water relations of *Robinia pseudoacacia* L.: do vessels cavitate and refill diurnally or are R-shaped curves invalid in *Robinia*?. Plant Cell Environ. 37: 2667–2678. https://doi.org/10.1111/pce.12315.

Wason JW, Huggett BA, Brodersen CR. 2017. MicroCT imaging as a tool to study vessel endings in situ. Am. J. Bot. 104: 1424–1430. https://doi.org/10.3732/ajb.1700199.

Wheeler JK, Sperry JS, Hacke UG, Hoang N. 2005. Inter-vessel pitting and cavitation in woody Rosaceae and other vesselled plants: a basis for a safety versus efficiency trade-off in xylem transport. Plant Cell Environ. 28: 800–812. https://doi.org/10.1111/j.1365-3040.2005.01330.x.

Associate Editor: Frederic Lens